SIMULATING MICROMETEOROID BOMBARDMENT ON MERCURY: IDENTIFYING NEW SPACE WEATHERING FEATURES IN THE LABORATORY. N. Bott[1], M. S. Thompson[1], K. E. Vander Kaaden[2], M. J. Loeffler[3] and F. M. McCubbin[4], [1]Department of Earth, Atmospheric, and Planetary Sciences, Purdue University, West Lafayette, IN, 47907, United States of America (nbott@purdue.edu), [2]NASA Headquarters, Mary W. Jackson Building, Washington, DC, 20546, United States of America, [3]Northern Arizona University, Flagstaff, AZ, 86011, United States of America, [4]ARES, NASA Johnson Space Center, Houston, TX, 77058, United States of America.

Introduction: Airless bodies are continually exposed to the harsh interplanetary space environment, causing the alteration of their surfaces through a process known as space weathering (SW) [1]. SW is dominated by solar wind irradiation and micrometeoroid bombardment, which together alter the spectral, microstructural, and chemical characteristics of grains on the surface of airless bodies. The effects of SW are variable and depend on the heliocentric distance and the initial composition of the planetary surface, among other factors [2]. On the Moon and S-type asteroids, it is well established that SW darkens and reddens the surface of these bodies and attenuates absorption bands across the Vis-NIR wavelengths. These spectral effects are largely the result of the production of metallic Fe nanoparticles (npFe). However, Mercury's SW environment is unique compared to the Moon and S-type asteroids. Mercury is a geochemical endmember, with a surface composition low in Fe (<2 wt.%) [3] and enriched in volatile components, including regions of the surface hypothesized to contain up to 4 wt.% graphite in the low reflectance material (LRM) [4]. In fact, the presence of graphite on Mercury has been hypothesized to act as a reducing agent for silicates during SW to produce Si-bearing Fe-rich metal [5]. In addition, its location in the solar system exposes Mercury to an extreme SW environment, with the surface of the planet experiencing an intense solar wind flux and higher flux and velocity of micrometeoroid impactors compared to the Moon and S-type asteroids [6]. The effects that such harsh SW has on materials with the unique compositional characteristics of Mercury are not well constrained. To better understand SW at Mercury, we must investigate these processes in the laboratory.

Here, we present the results of our analyses of the spectral, microstructural and chemical characteristics of Mercury analog samples irradiated by pulsed laser to simulate the short duration, high temperature events associated with micrometeoroid impacts.

Samples and methods: We prepared powdered samples (45–125 μm grain size) of synthesized forsteritic olivine at NASA Johnson Space Center (JSC) [7]. Several FeO contents representative of those at the surface of Mercury were prepared, including low-Fe samples F-T-004 (0.53 wt.% Fe) and F-S-002 (0.05 wt.% Fe). In addition, we employed a sample of SC-001 (San Carlos olivine, Fo_{90-91}, 9.01 wt.% Fe) for comparison with previous experiments [8]. Each sample was mixed with graphite (5 wt.%) to account for the high-carbon content of the LRM. The samples were pressed into pellets at Northern Arizona University (NAU). Finally, to simulate micrometeoroid impacts, the mixtures were irradiated with an Nd-YAG (λ=1064 nm) pulsed laser under ultra-high vacuum with a pulse duration of ~6 ns and an energy of 48 mJ/pulse. Each sample experienced progressive irradiation, first 1x, then 3x, and finally 5x laser rasters over the surface.

Infrared (0.65–2.5 μm) reflectance spectra of the samples were acquired using a Nicolet IS50 FTIR spectrometer at NAU. The surface morphology of the samples was analyzed by scanning election microscopy (SEM) using a FEI Nova NanoSEM200 and a Hitachi TM 4000 Plus benchtop equipped with Oxford energy dispersive x-ray (EDX) detectors at Purdue University. Finally, electron-transparent thin sections of the samples were prepared with a FEI Helios NanoLab 660 focused ion beam (FIB) at JSC for analysis with the FEI Talos 200X transmission electron microscope (TEM) equipped with a Super-X EDX detector at Purdue.

Results: Here we focus on the results of the SEM and TEM analyses.

SEM: Backscattered electron images and EDX chemical maps reveal no obvious chemical differences between the irradiated and unirradiated regions of the sample. The graphite is distributed homogeneously across the surface, and we identified fluffy carbon-rich deposits on the irradiated regions of the surface, along with regions with melt deposits for both low-Fe samples. We prepared FIB sections for both melt-rich and C-rich regions of the F-S-002 and F-T-004 samples for analysis in the TEM.

TEM: Characterizing the FIB section from the F-S-002 melt-rich sample revealed the presence of a 100 nm thick, amorphous melt layer at the surface [9]. Chemically, the melt layer shows an enrichment in Si and a complete depletion in Mg compared to the underlying olivine. Present within the melt layer were identified C-rich inclusions, ranging in size from 5-10

nm in diameter. Analyses are underway to determine their mineralogy (Figure 1).

In the FIB section prepared from the C-rich deposit of sample F-S-002, we have identified two distinct C-rich textures (vesiculated and fluffy) close to the surface of the sample, likely caused by laser irradiation [9]. We further investigated the former with HRTEM and EDS mapping (Figure 2).

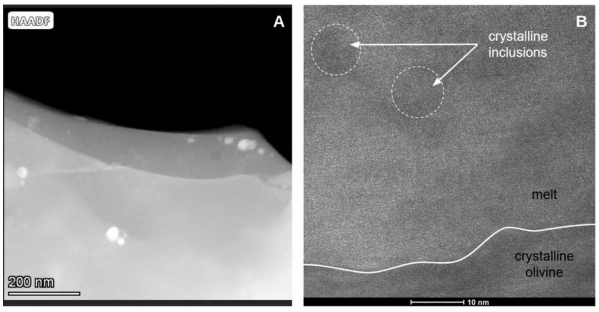

Figure 1: A. Scanning TEM (STEM) overview image of crystalline inclusions in the melt layer of the F-S-002 sample; B. High-resolution TEM (HRTEM) image of crystalline inclusions.

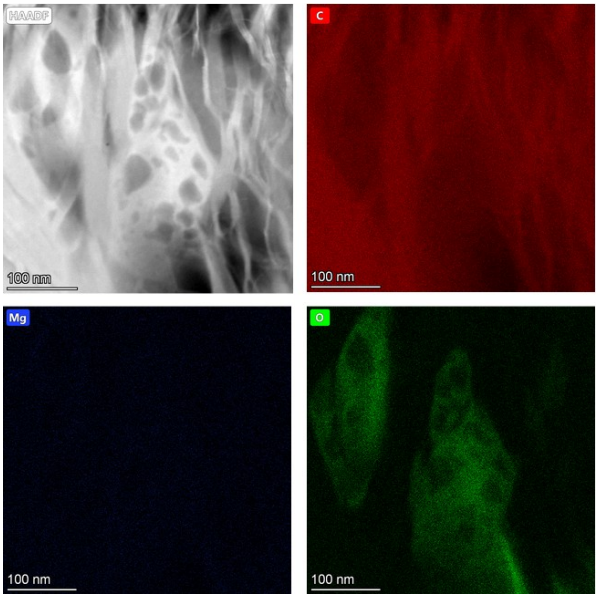

Figure 2: EDS mapping of a vesiculated olivine area enclosed in a carbon-rich region of the F-S-002 sample.

HRTEM images of the vesiculated textures and the surrounding material show amorphization. The EDS chemical mapping reveals that this material is richer in Fe, O and Si than the surrounding material, and that it is enclosed in a region richer in C. We note the entire region is completely depleted in Mg, similar to the compositional changes observed in the melt-rich deposit from the same sample [9]. Further investigation of the molecular ratio of Fe:Si of this vesiculated material should help to determine if it has an olivine-like or pyroxene-like composition. The same features (C-rich inclusions in the melt layer, vesiculated olivine in the C-rich phase) have been identified as widespread throughout the sample, suggesting they can be typical SW products at the surface of Mercury.

Discussion: The absence of npFe in the melt layer of the F-S-002 sample indicates that these particles are not formed (or in a very small amount) in materials with a very low-Fe content. On the contrary, the identification of vesiculated material richer in Fe, Si and O may be the result of the interaction of graphite with komatiites and boninites via smelting [5], although further analyses are needed to confirm the mineralogical nature of this material. Finally, the C-rich nanoinclusions present in the melt layer were predicted by spectral modeling, and they were also expected to form more easily than nanophase Fe [10].

Conclusion: Our analyses of laser irradiated Mercury analog samples enabled the identification of SW products specific to these low-Fe, C-rich compositions (e.g., vesiculated olivine, C-rich nanoinclusions). This confirms the high correlation between the initial composition of a surface and the effects of SW on its spectral, microstructural and chemical properties.

We will soon investigate other sample compositions (e.g., including sulfur instead of carbon) to better understand how the effects of SW could differ. We will also analyze the effects of solar wind irradiation on the spectral, microstructural and chemical characteristics of Mercury analogs using samples irradiated by H and He ions.

References:

[1] Pieters, C. M., and Noble, S. M. (2016) *JGR-Planets*, *121*, 1865-1884. [2] Lantz C. et al. (2017) *Icarus*, *285*, 43-57. [3] Nittler L. R. et al. (2011) *Science*, *333*, 1847-1850. [4] Klima R. L. et al., (2018) *Geophys. Res. Letters*, *45*, 2945-2953. [5] McCubbin, F. M. et al. (2017) *JGR-Planets*, *122*, 2053-2076. [6] Cintala, M. J. (1992) *JGR-Planets*, *97*, 947-973. [7] Thompson M.S. et al., *LPSC LII*, Abstract #2548. [8] Dukes C. A. et al. (1999) *JGR*, *104*, 1865-1872. [9] Bott N. et al., *EPSC 2022*, Abstract #574. [10] Trang, D. et al. (2017) *Icarus*, *293*, 206-217.